JTTEE5 9:49-58

Behavior of Plasma-Sprayed Thermal Barrier Coatings during Thermal Cycling and the Effect of a Preoxidized NiCrAlY Bond Coat

M.F.J. Koolloos and J.M. Houben

(Submitted 30 December 1998; in revised form 6 December 1999)

The failure mechanisms of thermal barrier coatings (TBCs) subjected to a thermal load are still not entirely understood. Thermal stresses and/or oxidation cause the coating to fail and hence must be minimized. During the present investigation, TBCs up to 1.0 mm were sprayed and withstood high thermal stresses during thermal testing. Owing to the substantial thickness, the temperature at the top coat/bond coat interface was relatively low, resulting in a low oxidation rate. Furthermore, bond coats were preoxidized before applying a top coat. The bond strength and the behavior during three different thermal loads of the preoxidized TBCs were compared with a standard duplex TBC. Finite-element model (FEM) calculations that took account of bond coat preoxidation and interface roughness were made to calculate the stresses occurring during thermal shock. It is concluded that the thick TBCs applied during this research exhibit excellent thermal shock resistance and that a preoxidizing treatment of the bond coat increases the lifetime during thermal loading, where oxidation is the main cause of failure. The FEM analysis gives a first impression of the stress conditions on the interface undulations during thermal loading, but further development is required.

Keywords plasma spraying, thermal barrier coatings, thermal cycling, bond coat oxidation, failure mechanism, finite element modeling, preoxidation, ZrO_2-Y_2O_3

1. Introduction

Thermal barrier coatings (TBCs) applied to the hot components of gas turbines experience very high heat fluxes. Owing to thermal stresses and oxidation of the bond coat, the lifetime is limited and failure occurs by delamination of the top coat.[1–4] Usually, this occurs just above the bond coat asperities. In previous work,[2] the influence of testing temperature on the failure mechanism was discussed. Moreover, it was shown that coating properties such as residual stresses, hardness, and phase composition changed due to heat treatment, but they were fairly independent of the test temperature. However, bond coat oxidation is enhanced by increasing temperature and is believed to be the main cause of delamination.[4] Oxidation of the bond coat can be diminished by lowering the interface temperature or by including an oxygen barrier between the top coat and the bond coat. An obvious way to decrease the interface temperature is to apply a thicker top coat. However, thick TBCs exhibit, in general, poor thermal shock performance.

Wigren *et al.*[5] and Bengtsson *et al.*[6] studied the thermal shock behavior of thick TBCs and found that good thermal shock resistance was obtained when the top coat contained vertical segmentation cracks, which lowered the top coat Young's modulus. An oxygen barrier can be achieved by preoxidizing the bond coat,[7] by use of a Chemical Vapor Deposition (CVD) Al_2O_3 layer,[8] or by applying a Vacuum Plasma Spray (VPS) Al_2O_3 layer.[9] The present research aims to lower the oxidation rate by applying both a thick top coat and an oxygen barrier. First, the behavior of TBCs with different thickness, up to 1 mm, is compared using three kinds of thermal loads. Second, the effect of a preoxidized bond coat is investigated.

The second part of this paper covers the modeling of the stresses that occur during thermal shock. Since the failure mechanisms of TBCs subjected to a thermal load are still not entirely understood, several finite-element models (FEMs) have been developed to predict the stresses at the top coat/bond coat interface and to elucidate the failure mechanism.[10,11,12] Chang *et al.*[10] predicted the stresses during only one cooling cycle, including oxidation but not creep. Tsui *et al.*[11] incorporated oxidation and creep and simulated 10 cycles of 1 h at 1000 °C with intermediate cooling to room temperature. Hence, their model calculated only the stresses during furnace testing. Freborg *et al.*[12] developed a very comprehensive model including bond coat roughness, creep, oxidation, and multiple thermal cycles. The model consisted of a small slice from a coated rod. They used a measured thermal profile with a heating period of 6 min followed by a forced air-cooling period of 4 min.

The purpose of the current work is to develop a model to calculate the stresses in a coated strip. The first step includes the calculation of the temperature and stress profile on a macroscale. The calculated temperature can be validated with the experiments for nodes at the surface of the top coat and at the rear side of the substrate. Next, the "global-local approach" is applied, whereby a small part of the global model is investigated by "cutting" that part from the global model, incorporating microgeometry such as bond coat roughness, refining the

M.F.J. Koolloos and **J.M. Houben,** Department Mechanical Engineering, Section Thermal Spraying, Eindhoven University of Technology, 5600 MB Eindhoven, The Netherlands. Contact e-mail:koolloos@nlr.nl.

elements, and applying the appropriate boundary conditions. The model is still in development and the results presented here are from the simulation of a short cycle thermal load by means of an elastic analysis without creep and oxide growth. The model indicates the influence of a preoxidizing treatment and the effect of a change in the bond coat Young's modulus and coefficient of thermal expansion (CTE) and the top coat Young's modulus.

2. Material and Coatings

2.1 Specimens

The materials used during this research and the spraying conditions for the bond coat and top coat are given in Table 1. The top coat was applied to thicknesses of 0.30, 0.68, and 1.0 mm. The spraying parameters used for the top coat combined with a water-cooled substrate resulted in a high deposition efficiency (about 60%) and a coating with a low porosity (<5%), a dense network of microcracks, low tensile stresses in the as-sprayed state (<50 MPa), and a high thermal shock and erosion resistance.[2]

2.2 Preoxidation of the bond coat

Before arriving at the final configuration of the specimens, it was necessary to conduct some initial experiments, in order to choose a preoxidation treatment for the bond coat. The procedure for this is schematically given in Table 2 and will be discussed in this section.

Bond coats were heat treated in a high-temperature furnace at 1325 K for 2.5, 5, 10, 25, and 50 h. Next, a cross section was embedded and examined *via* a scanning electron microscope (SEM, JEOL 8600 SX, Japan Electron Optics Ltd., Tokyo). From the SEM pictures, the oxide layer thickness was determined.

The phases and elements were determined to reveal the composition of the preoxidized layer. Phase analysis was done by x-ray diffraction, using a Rigaku Geiger Flex (Rigaku International Corporation, Tokyo, Japan) x-ray diffraction apparatus with a voltage of 35 kV and a current of 20 mA. Diffraction scans were run from 20 to 80° 2θ, with a scanning speed of 0.12° 2θ min^{-1}. The radiation used was Cu K_α. Chemical element analysis was performed by electron probe microanalysis on a JEOL 8600 SX with a voltage of 20 kV. For each measurement, a line scan was carried out with a step size of 2 μm, starting in the substrate and ending in the top coat. The elements O and Ni were determined by wavelength dispersive spectrometry (WDS), and the elements Al, Cr, Fe, and Mo by energy dispersive spectrometry (EDS). The chemical element analysis was also used to examine the influence of the preoxidation treatment on the bond coat composition. After inspection of the resulting oxide layer (Section 4.1), it was concluded that preoxidizing times of 5 and 10 h were eligible for further experiments. A 0.3 mm TBC was applied on the bond coats preoxidized for 5 h, and 0.3 and 0.68 mm TBC were applied on the bond coats preoxidized for 10 h.

The bond strength of the top coat on a preoxidized bond coat was compared with non-preoxidized TBCs. This was performed for both an as-sprayed and a heat-treated (1325 K/5 h) TBC system. The test specimen configuration is schematically given in Table 2. Small pieces 18 × 18 mm in size were cut out of the large coated strips with a diamond wire saw and glued on steel bars with a high strength adhesive (3M HT 2214, bond strength ~70 MPa). To avoid penetration of the adhesive into the porous top coat, the surface was first sealed with Metco AP sealer (Sulzer Metco AG, Switzerland). The bars were mounted in a 100 kN tensile testing machine with special gripping fixtures to avoid bending. The bond strength tests were performed at a crosshead rate of 2 mm min^{-1}. All specimens were tested twice.

Table 1 Specimen materials and spraying parameters for the bond coat and top coat

		Coating spray parameters					
Material	**Thickness (mm)**	**Ar flow rate (L/min)**	**H_2 flow rate (L/min)**	**Arc current (A)**	**Voltage (V)**	**PFR (a) (G/min)**	**Spray distance (mm)**
Hastelloy X substrate, 125 × 30 mm strip	3.2	. . .	. . .	. . .	. . .	. . .	. . .
NiCrAlY bond coat(b), Amperit 413.6(c)	0.1	46.8	8.2	500	58.2	50	100
ZrO_2-8wt.%Y_2O_3 top coat, Amperit 825.1	0.30 0.68 and 1.0	36.0	9.0	500	55.6	44	100

(a) PFR = powder feed rate. (b) As-sprayed and preoxidized (Table 2). (c) Chemical composition (wt%): 22Cr, 10Al, 1.0Y, balance Ni

Table 2 Preliminary investigations of as-sprayed and preoxidized bond coats

Purpose	**Method**
Preoxidizing bond coat	Furnace heat treatment at 1325 K for 2.5, 5, 10, 25, and 50 h
Morphology and thickness of oxidized layer (preoxidized only)	SEM
Phase composition	X-ray diffraction
Element composition	WDS EDS
Bond strength top coat	Tensile adhesion test

specimen set-up for tensile adhesion test

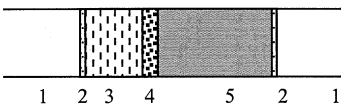

1: steel bars 2: adhesive
3: top coat* 4: bond coat
5: substrate
*surface sealed before adhesive bonding

The adhesion strength test described here is similar to the standardized DIN 50160 and ASTM C633 method, but it differs in the specimen preparation. The coatings of the standardized tests are directly sprayed onto (cylindrical) bars, which are rotated during the spraying process. Consequently, the relative tangential velocity is zero at the center of the specimen and maximum at the boundary. This results in varying deposition characteristics over the specimen surface and, hence, varying coating properties.

3. Experimental Investigation

An overview of the test program is given in Table 3. Details of the thermal test equipment and testing conditions are given in Sections 3.1 and 3.2.

3.1 Thermal Test Equipment

The TBCs were tested in a burner rig and in a high-temperature furnace. The burner rig locally heats the coating surface with an oxygen/acetylene flame. The rig is computer controlled and two specimens can be tested at the same time. The main parameters of the testing process are the surface temperature, T_{surf}, and the temperature at the rear side of the substrate, T_{subst}, both measured at the midpoint of the heated area. The T_{surf} is measured with an optical pyrometer and the T_{subst} with a thermocouple. Further details of the burner rig are published in Ref 2. The computer controlled furnace is equipped with a movable bottom, which consists of porous ceramic blocks, which are held by a Hastelloy X (Haynes International, Inc., Kokomo, IN, USA) band. The blocks have holes for placing test pins to support the samples. Heating of samples takes place with $MoSi_2$ heating elements, and cooling is induced.

Burner rig tests are essentially different from furnace tests. During burner rig testing, a large thermal gradient exists across the specimen thickness, resulting in a relatively low interface temperature. During furnace testing, the entire specimen is heated to a certain temperature and in general for longer time cycles. Consequently, degradation of the bond coat and substrate owing to oxidation and diffusion is more severe. Moreover, the large differences in thermal expansion between substrate, bond coat, and top coat, in combination with a homogeneous temperature, result in higher thermal stresses during cooling. In order to obtain similar oxidation circumstances for the bond coat, and hence to make a comparison of the results of the furnace tests and the burner rig tests meaningful, the applied testing temperatures were chosen in such a way that the bond coat temperature was similar for both tests.

3.2 Test Conditions

Two kinds of thermal load were performed with the burner rig: a short cycle and a long cycle. In the first, hereafter referred to as thermal shock, the specimens were heated in 28 s to a maximum T_{surf}. This temperature was varied from 1575 to 1725 K in order to investigate its effect on the failure mechanism. The maximum temperature on the rear side of the substrate depended on the coating thickness and varied between about 300 K lower than T_{surf} for a 0.3 mm thick top coat to 550 K lower for a 1 mm thick top coat. After the heating period, the specimens were cooled over the entire coating surface for 28 s, at which T_{subst} reached its lowest value of about 675 K. After each 100 cycles, the specimens were cooled to room temperature to simulate gas turbine shutdown.

During the second kind of thermal load, hereafter referred to as thermal cycling, test specimens were heated for 60 min. After a short transient period, a steady state was reached with T_{surf} = 1625 K. The thermal cycling tests were performed only with the 0.3 mm thick TBCs, in which case T_{subst} was about 250 K lower than T_{surf}. After the heating period, the specimens were cooled for 1 min to T_{subst} = 495 K.

During the furnace tests, the samples were heated up to 1410 K in 4 min and held at this temperature for 50 min. Next, they were cooled to 575 K in 6 min. After every 20 cycles, the samples were held at room temperature for 4 h. During this period, they were thoroughly inspected for signs of failures.

The burner rig tests were aborted if delamination of the top coat occurred in the area covered by the flame. The test was also stopped if no damage had occurred after 5000 cycles. The criterion for failure and removal of the furnace test samples was 10% delamination of the top coat. In addition, the failed furnace test samples were subjected to a chemical analysis on the bond coat to reveal its high-temperature degradation.

Since thermal testing of TBCs is a very time-consuming process, and many different coatings were tested, the number of duplicate experiments was kept small (Table 3). Most experiments were carried out twice or more, but when the trend was clear for the same kind of experiment, only one sample was tested. This was the case for determination of the influence of preoxidation treatment time (5 versus 10 h), which was evaluated for thermal shock, thermal cycling, and furnace tests. It was also the case when the thick coatings did not fail and for the thermal cycling tests.

4. Experimental Results

4.1 Properties of Preoxidized Bond Coat

The preoxidizing treatment of the bond coat resulted in a <1 μm (2.5 h), 1.5 ± 0.25 μm (5 h), 2.0 ± 0.5 μm (10 h), and 2.5 ± 0.5 (25 and 50 h) thick oxide layer. The oxide scale after 2.5 h did not cover the complete surface and was hence unusable for a

Table 3 Survey of main investigation

Top coat thickness (mm)			**0.30**			**0.68**		**1.0**
Preoxidation time (h)			**0**	**5**	**10**	**0**	**10**	**0**
Type of test,	Thermal shock	1575	2	. . .	. . .	. . .	. . .	1
test temperature (K),		1625	2	1	1	. . .	. . .	. . .
and number of specimens		>1675	4	. . .	. . .	1	2	1
	Thermal cycling	1625	1	1	1	. . .	. . .	. . .
	Furnace testing	1410	3	1	1	2	2	1

TBC system. After 5 and 10 h preoxididation, a dense uniformly thick scale was formed (Fig. 1) for a 10 h preoxidized bond coat. Longer preoxidation treatments resulted in dense oxide scales, which were partly cracked or spalled. Moreover, severe internal oxidation had occurred.

From the phase analysis, it was found that for the preoxidation treatments of 2.5, 5, and 10 h, the oxide scale consisted predominantly of α-Al_2O_3 (*e.g.*, Fig. 2 for 10 h). Small amounts of other oxides such as NiO and spinel type structures (*e.g.*, $NiAl_2O_4$) were also observed. Preoxidation treatment for 25 and 50 h resulted in more of these oxides and spinel type structures compared to α-Al_2O_3. Since this is detrimental to the thermal shock resistance,[7] the bond coats used during the present research were preoxidized for 5 and 10 h.

The results from the elemental analysis supported the observation that the oxide layer consisted predominantly of α-Al_2O_3. Figure 3 shows the composition of a bond coat of local thickness 52 μm and preoxidized for l0 h. At the oxide location, a strong increase in A1 (from 8 to about 40 wt.%) and a decrease in Cr and Ni were observed. The preoxidation heat treatment resulted in a decrease of the bond coat bulk content of Ni and Al and an increase in the amount of Cr.

The bond strength data exhibited a lot of scatter in Fig. 4. Despite this, a slight decrease of bond strength of the top coat (8% in the as-sprayed state and 13% in the heat-treated state) owing to preoxidation could be observed.

4.2 Number of Cycles to Failure during Thermal Loading

The results of the thermal shock tests are given in Fig. 5, which indicates the number of cycles to failure for several maximum surface temperatures and for each coating thickness. Photographs of the damage before and after delamination of the top coat are given in Ref 2. Most coatings failed by complete delamination in the top coat material just above the interface asperities and in the area covered by the flame. The exceptions were the following: at T_{surf} = 1625 K, both the non-preoxidized and preoxidized 0.3 mm specimens failed due to severe degradation of the substrate and bond coat without top coat delamination; and at T_{surf} = 1675 K, the 0.3 mm specimen failed due to top coat degradation, resulting in partial delamination,[2] and the 0.68 and 1.0 mm specimens without preoxidizing did not fail. These tests were stopped after 5000 cycles, except for the 1.0 mm specimen tested at 1775 K, which was stopped after 3000 cycles.

The 0.68 mm TBCs with a preoxidized bond coat failed by delamination after 2500 cycles. Also, a large piece of the top coat contiguous to the area covered by the flame was removed by spalling. Moreover, delamination occurred more at the interface instead of in the area just above the asperities. Since the specimen tested at 1625 K failed due to substrate and bond coat degradation, no difference between the 5 and 10 h preoxidation treatment could be indicated. Microscopic investigations on the thick coatings, which were not delaminated, revealed that vertical segmentation cracks formed that did not reach the bond coat. Also, at the area covered by the flame, some small horizontal cracks were formed just above the interface.

The results for the thermal cycling and furnace tests of the 0.3 mm TBCs are shown in Fig. 6, which presents the average

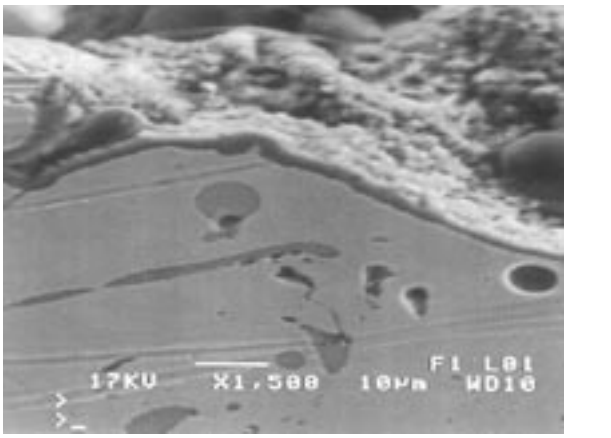

Fig. 1 SEM micrograph of cross section of preoxidized (1325 K/10 h) NiCrAlY bond coat

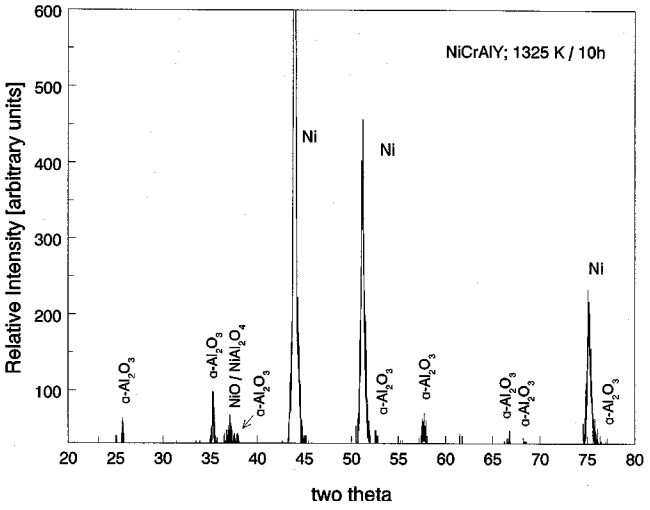

Fig. 2 Diffraction pattern of a preoxidized (1325 K/10 h) NiCrAlY bond coat

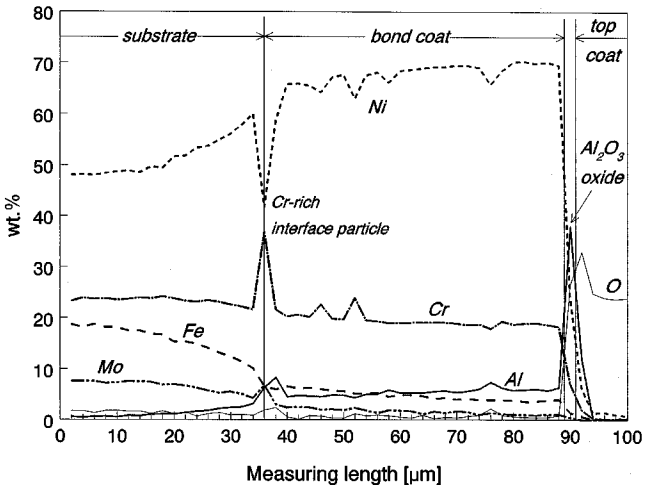

Fig. 3 Chemical element analysis of a preoxidized (1325 K/10 h) NiCrAlY bond coat. The bond coat has a local thickness of 52 μm

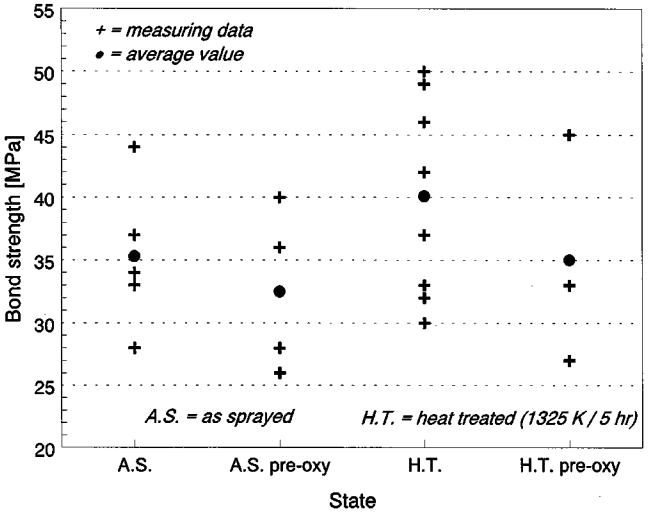

Fig. 4 Influence of preoxidation and heat treatment (1325 K/5 h) on bond strength of top coat

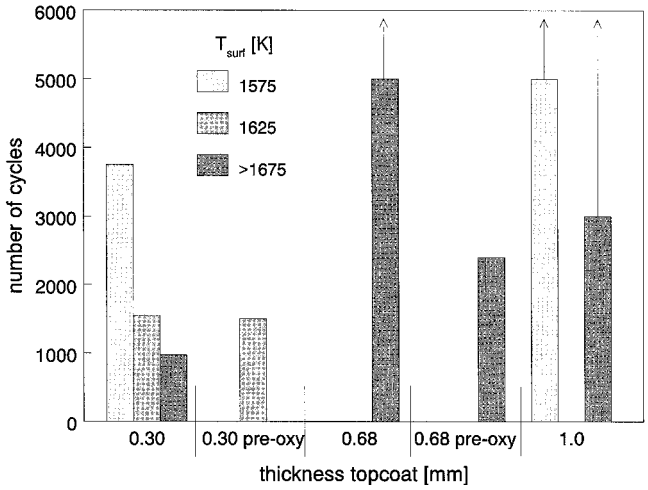

Fig. 5 Number of thermal shock cycles to failure for several test temperatures and for 0.3 and 0.68 mm (with and without preoxidized bond coat) and 1.0 mm specimens. The arrow on top of the bar indicates that delamination did not occur within the given number of cycles

results of the 5 and 10 h treatments for the preoxidized specimens.[1] For the thermal cycling tests, an increase in lifetime of about 25% was achieved by applying a preoxidized bond coat (115 versus 92 cycles). For the furnace tests, a considerable increase in cycles to failure was obtained by using a preoxidized bond coat (440 versus 300 cycles). The results of the thick coatings are not shown in Fig. 6, since failure occurred after only a few cycles. The 0.68 and 1.0 mm specimens without preoxidation treatments all failed within 20 cycles and the preoxidized 0.68 mm coating failed after 40 cycles. All failures from the thermal cycle and furnace tests occurred by delamination of the top coat in the same way as during thermal shock. There was no difference in the location of delamination observed between the TBCs with a preoxidized and an initial nonoxidized bond coat. Figure 7 shows a detail of the interface region of a nondelaminated part of a 0.3 mm thick TBC after 300 furnace cycles. An oxide layer of about 10 μm was formed and small horizontal cracks had formed in the top coat just above the interface. The chemical element analysis of the furnace-tested bond coats showed that depletion of Ni and Al and enrichment of Cr, Fe, and Mo in the bond coat had occurred. The level of these elements was the same in the substrate near the interface and the bond coat. The bulk content of Al was reduced from 10 wt.% in the as-sprayed state to 2 wt.% after 300 cycles.

[1] The difference in results between 5 and 10 h preoxidation was negligible for both thermal cycling and furnace tests. Delamination occurred after 116 (5 h) and 115 (10 h) cycles for thermal cycling, while the specimens tested in the furnace failed after 450 (5 h) and 430 (10 h) cycles.

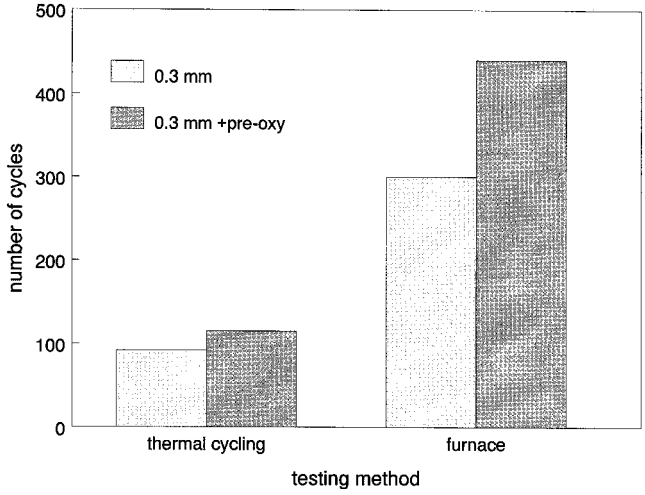

Fig. 6 Number of cycles to failure during thermal cycling and furnace testing, for 0.3 mm specimens with and without preoxidized bond coat

5. Finite Element Modeling of Thermal Shock

5.1 Global Model

The thermal shock test of a specimen was simulated by an axisymmetric, elastic, uncoupled thermomechanical analysis, using the MARC (MARC Analysis Research Corporation, Palo Alto, CA, USA) code. A disc-shaped specimen with a diameter of 30 mm was modeled. The calculation covers a time period of 90 s, *i.e.*, 30 s heating, 30 s cooling, and 30 s heating. The heat input from the flame is modeled as a circular flux 14 mm in diameter, applied at the top coat surface in the specimen center. The heat transfer coefficient of the flame (h_{flame}) was determined semiempirically. First, the heat flow from the burner to the specimen (Q_{in}) was determined from the steady-state temperature profile over a coated specimen:

$$Q_{in} = \frac{\Delta T}{(d/\lambda)_{tc} + (d/\lambda)_{bc+\text{subst}}} \left(\text{W m}^{-2}\right) \quad \text{(Eq 1)}$$

where ΔT is the measured temperature difference between T_{surf} and T_{subst}, d is the thickness, and λ is the conductivity. The subscript *tc* indicates the top coat. The subscript *bc* + subst indicates the bond coat + substrate. Since the bond coat thickness is relatively small, the bond coat and substrate are considered as one

material with the conductivity property of the substrate. The term Q_{in} consists of the convective heat input from the flame minus the radiation to the surroundings. Assuming a flame temperature of 2500 K, h_{flame} can then be calculated according to

$$h_{flame} = \frac{Q_{in} + \sigma\varepsilon\left(T_{surf}^4 - T_\infty^4\right)}{T_{flame} - T_{surf}} \left(W\,m^{-2}\,K^{-1}\right) \quad \text{(Eq 2)}$$

where σ is the Stefan–Boltzmann constant, ε is the emissivity of the top coat (assumed to be 0.75), T_{surf} is the surface temperature of the coating, and $T\infty$ is the surrounding temperature. The value thus obtained (2200 W m^{-2} K^{-1}) is valid only at the steady-state surface temperature (1800 K). The dependency of h_{flame} on T_{surf} is analytically determined from the theory of an impinging jet.[13] In this way, the following equation is obtained:

$$h_{flame} = 2200 \cdot f(T_{surf}) \quad \left(W\,m^{-2}\,K^{-1}\right) \quad \text{(Eq 3)}$$

where $f(T_{surf})$ is a third-degree polynomial function, which varies between 0.92 for T_{surf} = 300 K and 1.0 for T_{surf} = 1800 K. Cooling of the specimen was assumed to occur, as in the tests, over the entire top coat surface. The heat transfer coefficient of the cooling jet (h_{cool} = 400 W m^{-2} K^{-1}) was determined from the calculations by trial and error, knowing that the experimental substrate temperature at the end of the cooling period was about 650 K. Further boundary conditions for the thermal analysis were radiation at the coated side and radiation and free convection (h = 15 W m^{-2} K^{-1}) at the rear side of the substrate. The calculated temperature profile was applied as a load for the structural analysis.

The thermophysical and elastic material properties, adopted for the FEM analysis, are given in Table 4. These values were taken from the literature and included temperature dependence if such data were available. When the literature data were in tabular form, they were fitted to the equations given in Table 4. Since there is no consensus about the CTE, Young's modulus, and Poisson's ratio of the top coat and the Young's modulus of the bond coat, averages from literature values are used. The top coat Young's modulus is assumed to decrease from 25 GPa at room temperature to 12 GPa at 1800 K.

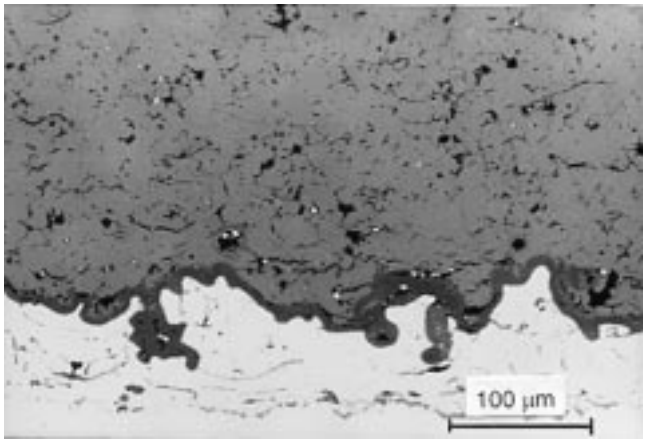

Fig. 7 Cross section of the interface region of a 0.3 mm TBC after 300 furnace cycles of 50 min at 1410 K

5.2 Global-Local Approach

In order to analyze stresses near the bond coat/top coat interface, a detailed mesh of this region was made. A small piece with a radius of 0.2 mm was excerpted from the global model. Next, a new fine mesh was generated, including a rough interface simulated by a sine wave with an amplitude of 30 μm and wavelength of 130 μm. These values were selected on the basis of roughness measurements and microscopic observations. At the interface, a 5 μm thick layer existing of very fine elements with a thickness of 1 μm was added to enable incorporation of an oxide layer. Figure 8 presents details of the FEM mesh at the interface region.

At the junction of the global and local models, the appropriate time-dependent boundary conditions obtained from the global model must be applied to the nodes of the local model. For the thermal analysis, the heat flow in the radial direction is used and the radial displacements are used for the structural analysis. Since this is a very time-consuming process, it was decided as a first approximation to apply one average time-dependent boundary condition to all nodes at the junction of the local model.

With the local model, the stresses perpendicular to the interface were calculated. Five cases were run. First, the material properties as given in Table 4 were used. The small elements allocated to the alumina layer were given bond coat properties. In the four following cases, the influences of the bond coat Young's modulus (from 80 to 160 GPa), the bond coat CTE (from $12.5\cdot10^{-6}$ to $16.0\cdot10^{-6}$ K^{-1}), and the top coat Young's modulus (100% increase) and the presence of a 5 μm thick oxide (Al_2O_3) layer between the top coat and the bond coat were examined. For this last case, the alumina layer was assumed to have no effect on the temperature profile and only a stress analysis was performed.

6. FEM Analysis Results

6.1 Global Model

The temperature profiles at the top coat surface and substrate rear side at the center of the flame are shown in Fig. 9. The initial increase of T_{surf} was considerable. The final value after the

Table 4 Thermophysical and elastic materials properties, used for the FEM analysis

Property	Unit	Top coat	Bond coat[9]	Substrate[14]	Oxide[16]
Thermal conductivity, λ	W m^{-1} K^{-1}	$0.4384 + 12.78\cdot10^{-4}\,T$[9]	$8.57 + 0.01143\,T$	$3.573 + 1.99.10^{-2}T$	. . .
Specific heat, c_p	J kg^{-1} K^{-1}	$566.0 + 6.123\cdot10^{-2}T - 1.143\cdot10^{7}\,T^{-2}$[15]	488.9	$444.8 + 15.6e^{(T/416.16)}$	. . .
Density, ρ	kg m^{-3}	5760[9]	6668	8220	3950
CTE, α	K^{-1}	$10.8\cdot10^{-6}$(a)	$12.5\cdot10^{-6}$	$16.3\cdot10^{-6}$	$7.9\cdot10^{-6}$
Young's modulus, E	GPa	$27.6 - 8.67\cdot10^{-3}T$(a)	80(a)	$220.0 - 7.241\cdot10^{-2}T$	387
Poisson's ratio, ν	—	0.2(a)	0.31	0.32	0.3

(a) Average from values reported in the literature

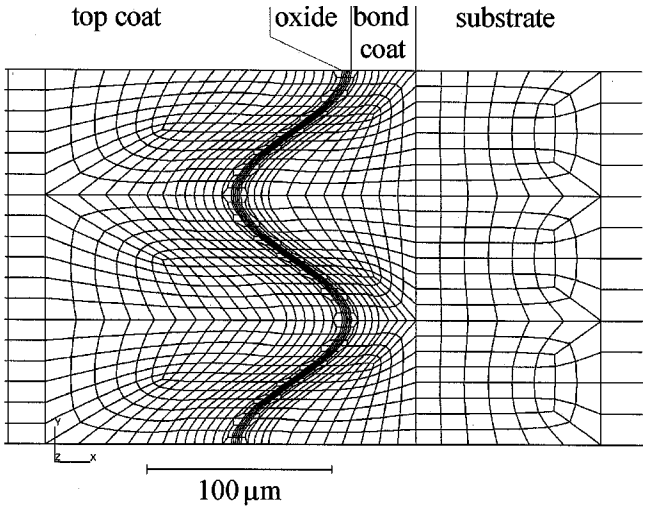

Fig. 8 FEM mesh of interface region

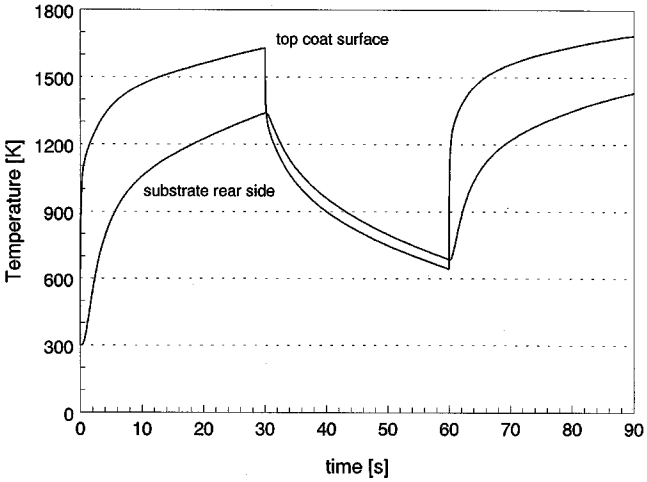

Fig. 9 Calculated temperature profile at the center of the specimen for the top coat surface and substrate rear side

first heating period was 1629 K for T_{surf} and 1339 K for T_{sub}. After cooling, T_{surf} was 643 K and T_{subst} was 686 K. The temperatures after the second heating period were higher than after the first: T_{surf} was 1687 K and T_{subst} was 1431 K.

The calculated in-plane radial stresses at the center of the flame are shown in Fig. 10. The given locations were at middepth of the top coat and in the substrate at 2 mm from the substrate/bond coat interface. At the beginning of the heating period, the stresses in the coating were compressive and reached a maximum value of about 100 MPa. Halfway through the heating period the stress became tensile. The tensile stress increased more during cooling. At the beginning of the second heating period, the stress strongly decreased and even became compressive, but then reversed after a few seconds into a tensile stress as before. At the surface of the top coat (not shown in Fig. 10), the maximum stresses were all somewhat larger, but the tendency was the same. Outside the flame area, only tensile stresses prevailed at the coating surface.

The stresses in the substrate were compressive and were very high during the first 10 s of a heating period, especially during

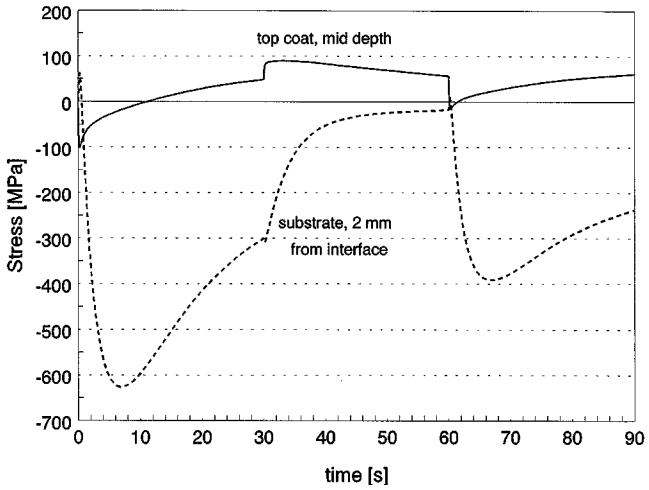

Fig. 10 Calculated in-plane radial stresses at the center of the specimen for a location at the middepth of the top coat and in the substrate at 2 mm from the interface with the bond coat

the first heating period. The highest compressive stresses occurred in the area just beneath the interface with the bond coat (this is also not shown in Fig. 10). The stresses diminished in the radial direction and toward the free surface of the substrate. When the specimen was cooled, the substrate stresses decreased rapidly almost to zero.

6.2 Local Model

Figure 11 shows the out-of-plane stresses in the top coat near an interface peak. In the first calculation (indicated as "reference" in Fig. 11), low compressive stresses developed. When the Young's modulus of the top coat was increased by 100%, the stresses increased by about 50%. A change in the Young's modulus of the bond coat (not shown in Fig. 11) did not have any effect. The influence of the bond coat CTE was larger: a CTE increase of almost 30% resulted in a stress increase of more than 100%. The most remarkable result was obtained when a 5 μm thick oxide layer between the top coat and the bond coat was modeled. In this case, the stresses near the interface peak underwent a reversal and became completely tensile.

The out-of-plane stresses in the top coat in a valley between interface peaks were opposite in sign and similar in magnitude to the stresses at the peaks (these valley stresses are also not shown in Fig. 11). Thus, when the material properties were changed or an oxide layer added the interface valley stresses followed the same trend –but reversed in sign– as the interface peak stresses.

7. Discussion

7.1 Experiments

The effect of an increased top coat thickness (0.68 and 1.0 mm) during thermal shock was obvious. First, at T_{surf} = 1575 K, the thick coatings did not fail within 5000 cycles while the 0.3 mm TBCs failed after 3700 cycles. Second, at T_{surf} = 1675 K, top coat degradation occurred for the 0.3 mm specimens, but not for the

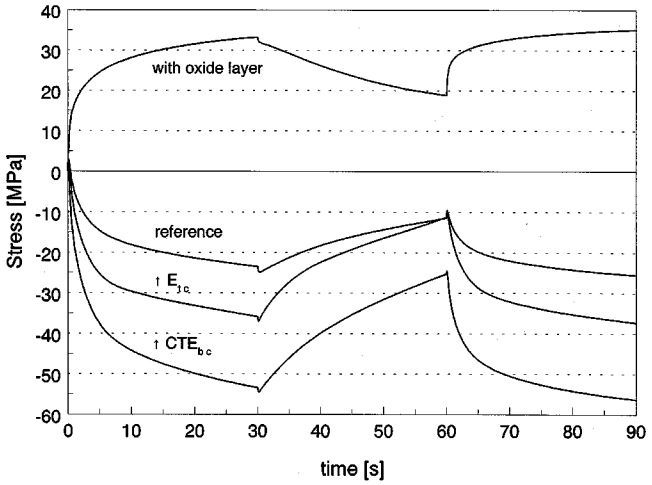

Fig. 11 Calculated out-of-plane stresses in the top coat near an interface peak. The effect of adding an oxide layer and the effect of an increase in top coat Young's modulus (E_{tc}) and bond coat CTE are also shown

thicker coatings. Finally, no sign of substrate and bond coat degradation was observed for the 0.68 and 1.0 mm top coats, while for the 0.3 mm coating, the test was stopped owing to severe degradation of the bond coat and substrate. The main reason for these results is that an increase in top coat thickness results in a decrease of the interface temperature, and hence lower oxidation rates, for the same T_{surf}. In addition, the top coat has a high strain tolerance owing to the microcrack network. Wigren *et al.*[5] and Bengtsson *et al.*[6] tested their TBCs at the same T_{surf} (1675 K) and found good thermal shock resistance owing to a segmented top coat. Wigren *et al.*[5] concluded that the optimum TBC contains a low percentage of microcracks, which contradicts the current results. However, they attributed the microcracks to poor adhesion between splats owing to poor particle melting. The spraying parameters applied during the present program resulted in well heated particles[17] and microcracking originated during substrate cooling only. Apparently, the thermal shock resistance is not unambiguously correlated to the microcrack density, but is affected by other microstructural properties as well.

Thick coatings give very poor results when the entire specimen is heated (furnace testing). Since the temperature of the substrate is much higher than in the case of thermal shock or thermal cycling, the effect of the difference in CTE between top coat and substrate is more severe for furnace testing, and this appears to be detrimental for thick coatings. The provisional conclusion of Tsui and Clyne[9] that delamination during furnace testing is due more to severe embrittlement of the region around the interface as oxidation occurs, rather than to a buildup of large driving forces, does not seem correct. If this were so, the difference in furnace testing performance between thick and standard 0.3 mm TBCs would not be as large as reported here. However, regarding Fig. 7, it seems very likely that embrittlement of the top coat during thermal cycling also plays an important role in the failure mechanism.

The effect of the testing temperature on the failure mechanism during thermal shock testing was observed only for the 0.3 mm top coats. Since at high temperatures top coat degradation did not occur for the thicker TBCs, it appears that the thickness of the top coat has a beneficial effect on the stress state in the outer layer. This will be investigated with the developed model in the future.

Table 5 Time at high temperature for three different thermal loads of 0.3 mm TBCs

Testing method	Average number of cycles to failure	Heating period (min)	Total time (h)
Thermal shock	4000	0.5	33(a)
Thermal cycling	100	60	100
Furnace testing	300	55	275

(a) Time of complete heating period

In Table 5, the total times at high temperature before failure occurred are given for the three testing methods for the 0.3 mm coatings. The time-based life was highest in the case of furnace testing and lowest in the case of thermal shock experiments. For the latter, the time of the complete heating period is given. The total time at high temperature was even shorter than the 33 hr. given in Table 5 since the initial, relatively cold, heating time was included. As mentioned in Section 3.1, the bond coat temperature was almost the same for all three thermal loads. In fact, during the burner rig experiments, this temperature, which was determined from the FEM analysis, was even higher than during the furnace tests (1475 versus 1410 K). This indicates that introducing a three-dimensional stress gradient under constant oxidation conditions decreases the life considerably.

It must be mentioned that furnace tests are not realistic, since in gas turbines, the hot components are always heated at the coated side and often deliberately cooled at the substrate side. The reason furnace tests are still widely used is that they are relatively easy and they provide insight with regard to the oxidation resistance of the TBC system. It is more useful to employ thermal shock tests, where thick coatings performed very well. Still, the better and most realistic experiment is thermal cycling, where the failure mechanism lies between those of thermal shock and furnace testing. It is hence concluded that failure of a TBC in a realistic environment is very clearly due to an interaction of thermal stresses and bond coat oxidation and that the effect of oxidation must not be overestimated.

From the element analysis of the preoxidized bond coat and the bond coat of the furnace-tested TBC systems, it was found that the Ni, Cr, Al, Fe, and Mo levels in the substrate near the interface and the bond coat approached the same concentration owing to a heat treatment. This leveling out of initial and short time heat-treated concentration differences must therefore be due to diffusion processes. Moreover, diffusion must have been responsible for the formation of alumina at the top coat/bond coat interface and, hence, the low level of Al (2 wt.%) in the bond coat after furnace testing. It is suggested that the life of TBCs during furnace tests is also influenced by the rate at which the bond coat decomposes, especially Al depletion. In this light, a thicker bond coat is preferred to a thin one.

A preoxidation treatment for the bond coat must be long enough to form a dense alumina scale, but short enough to avoid the formation of spinel-type structures and excessive depletion of Al.[7] Then, preoxidation has a beneficial effect in the case of thermal loading where oxidation plays an important part in the cause of failure, *i.e.*, thermal cycling and furnace testing. The alumina layer acts as an oxygen barrier from the very first heating cycle. Moreover, during preoxidation, the initial rapid growth of the

oxide layer does not occur between the top coat and bond coat, so this induces no extra stresses. The improved performance during furnace testing of TBCs with a preoxidized bond coat was also reported by Lih *et al.*[7] However, when thermal stresses become more important (thermal shock), preoxidation decreased the lifetime. Since delamination of the top coat is enhanced by tensile stresses perpendicular to the interface,[10,12] the negative influence of preoxidation can be explained by the measured lower bond strength for TBCs with a preoxidized bond coat. Also, from the modeling results (Section 6.2), it was seen that an alumina layer between the bond coat and top coat detrimentally converted the stresses at the interface peaks from compressive to tensile. Since for thermal cycling and furnace testing the number of heating cycles was far less than for thermal shock, the beneficial effect of a lower oxidation rate owing to preoxidation was larger than the negative influence of a lowered bond strength and (higher) tensile stresses. This resulted in the longer life of preoxidized TBCs during thermal cycling and furnace testing.

7.2 Modeling

The differences between T_{surf} and T_{subst} after the first and second heating periods were only 60 and 90 K, respectively, whereas the temperature at the beginning of the second heating period was almost 400 K higher than at the beginning of the first heating period. This indicates that the maximum temperatures will probably converge within a few cycles to values close to those after the second heating period. This was in fact observed during the experiments.

The calculated temperatures of the coating and the substrate rear side at the end of the second heating period lay within the temperature range of the thermal shock experimental program, but the temperature difference between the surface and substrate was slightly lower. However, this discrepancy is minor considering that the numerical approach had to use material properties from the literature. If the same calculations were to be performed with a slightly different heat transfer coefficient and material properties, the experiment and simulation would match. The initial heating rate according to the global model was higher than during the experiments. However, a reliable analytical model based on the heating rate of a semi-infinite wall gave the same results for the first few seconds as the numerical model. It is possible that the measured initial heating rate deviated from the real situation owing to a measuring delay in the thermocouples.

The in-plane stresses in the top coat were mainly tensile. This explains the large vertical cracks that were observed, especially outside the flame area.[2] With respect to the substrate, the large compressive stresses exceeded the yield strength of Hastelloy X,[14] and it may be expected that the substrate would plastically deform. It was indeed observed that the specimens thermally shocked to T_{surf} = 1625 K were bent and that the substrate thickness had increased in the area covered by the flame.

The temperature calculated with the local model agreed well with that of the global model. The temperature front was hardly influenced by the asperities. However, the radial stresses did not agree with those from the global model: the trend was the same but the maximum compressive stress in the substrate was about 40% higher for the local model. This discrepancy arose because the local model used the average displacement in the radial direction. This shows that the boundary conditions in the structural analysis must be applied very accurately with respect to time and position. A procedure to automatically convert the calculated displacements from the global model to boundary conditions for the local model is being developed.

The local model has shown that stress concentrations occur at the interface peaks and valleys. Assuming that the inaccuracies in the radial stress values have no influence on whether the stresses perpendicular to the interface are tensile or compressive, then the stresses at the peaks are compressive and the stresses in the valleys are tensile. However, to cause delamination, the stresses at the peaks should be tensile.[10,12] This was achieved for the case of an oxide layer between the top coat and bond coat. Since the influence of the underlying material's Young's modulus on the out-of-plane stresses in the top coat is negligible, the change in stress from compressive to tensile is attributed to the lower value of the oxide CTE. As discussed in Section 7.1, this reversal can explain the poor performance of the preoxidized TBCs during thermal shock. Freborg *et al.*[12] found that the peak stresses did not reverse but became even more compressive owing to bond coat oxidation. However, they incorporated a thermally growing oxide layer, which induces compressive stresses owing to the volume increase (simulated by an artificially high CTE). Apparently, the effect of a preoxidized oxide layer on the stress state differs significantly from the effect of a growing oxide layer.

With the current model, it is not yet possible to elucidate the failure mechanism of TBCs during thermal shock (peak-to-peak cracking). However, the reversal of the peak stresses to tensile owing to an oxide layer and the expectation that creep behavior of the top coat and bond coat modifies the interface stresses substantially[12] is encouraging for further development of the model.

8. Conclusions

The experimental part of this investigation leads to the following conclusions.

- Thick TBCs developed during the current research program have excellent thermal shock resistance. This is directly due to the high strain tolerance provided by the microcracks in the top coat. Indirectly, the thermal shock resistance is provided by the inherent effect of top coat thickness lowering the interface temperature and, hence, the oxidation rate.
- Failure of TBCs under a thermal load is caused by a combination of thermal stresses and bond coat oxidation. The latter needs not necessarily be the primary cause of failure.
- Preoxidation of the bond coat has a beneficial effect on lifetime in the case of a thermal load where oxidation is the main cause of failure. The preoxidation time and temperature must be chosen such that a dense alumina layer is formed and the forming of spinel-type structures is avoided.

From the FEM analysis of thermal shock, the following conclusions are drawn.

- The global-local approach proves satisfactory for investigating the stress state at the interface region. However, mechanical boundary conditions obtained from the global model must be applied very accurately.

- Oxidation of the bond coat turns the stresses at the bond coat/top coat interface peak regions from compressive to tensile, and this probably enhances delamination.
- To understand the failure mechanism of TBCs, further development of the model is required. In the near future, creep in the top coat and bond coat, and a more realistic interface roughness will be added to the model. When these features are implemented, the analysis will also be performed for thermal cycling and furnace testing. Also, the influence of a top coat thickness of 1 mm will be investigated.

Acknowledgments

The authors gratefully acknowledge the National Aerospace Laboratory NLR of The Netherlands, for support during the modeling, and the Interturbine Coating Center (Lomm, The Netherlands), for the furnace tests.

References

1. R.A. Miller and C.C. Berndt: *Thin Solid Films*, 1984, vol. 119, pp. 195-202.
2. M.F.J. Koolloos, G.G. van Liempd, and J.M. Houben: *Surf. Eng.*, 1998, vol. 14 (2), pp. 144-48.
3. R.A. Miller and C.E. Lowell: *Thin Solid Films*, 1982, vol. 95, pp. 265-73.
4. W.J. Brindley and R.A. Miller: *Surf. Coating Technol.*, 1990, vol. 43/44, pp. 446-57.
5. J. Wigren, J.F de Vries, and D. Greving: in *Thermal Spray: Practical Solutions for Engineering Problems*, C.C. Berndt, ed., ASM International, Materials Park, OH, 1996, pp. 275-84.
6. P. Bengtsson, T. Ericsson, and J. Wigren: *J. Thermal Spray Technol.*, 1998, vol. 7, pp. 340-48.
7. W. Lih, E. Chang, B.C. Wu, and C.H. Chao: *Oxid. Met.*, 1991, vol. 36, pp. 221-38.
8. J.H. Sun, E. Chang, B.C. Wu, and C.H. Tsai: *Surf. Coating Technol.*, 1993, vol. 58, pp. 93-99.
9. Y.C. Tsui and T.W. Clyne: in *Thermal Spray: Practical Solutions for Engineering Problems*, C.C. Berndt, ed., ASM International, Materials Park, OH, 1996, pp. 275-84.
10. G.C. Chang, W. Phucharoen, and R.A. Miller: *Surf. Coating Technol.*, 1987, vol. 30, pp. 13-28.
11. Y.C. Tsui, R.C. Reed, and T.W. Clyne: *Proc. 1st United Thermal Spray Conf.*, C.C. Berndt, ed., ASM International, Materials Park, OH, 1998, pp. 267-76.
12. A.M. Freborg, B.L. Ferguson, W.J. Brindley, and G.J. Petrus: *Mater. Sci. Eng.*, 1998, vol. A245, pp. 182-90.
13. F.P. Incropera and D.P. DeWitt: *Fundamentals of Heat and Mass Transfer*, 3rd ed., John Wiley & Sons, New York, NY, 1990, pp. 431-38.
14. J.R. Kattus: in *Aerospace Structural Metals Handbook, vol. 4*, F.B. William, H. Mindlin, and C.Y. Ho, eds., CINDAS/USAF CRDA Handbooks Operation, West Lafayette, IN, 1996, code 4112, pp. 1-23.
15. H.L. Schick: *Thermodynamics of Certain Refractory Compounds, Vol. 1*, Academic Press, New York, NY, 1966, pp. 2.266.
16. H.E. Evans, A. Strawbridge, R.A. Carolan, and C.B. Ponton: *Mater. Sci. Eng.*, 1997, vol. A225, pp. 1-8.
17. A.T.J. Verbeek: Ph.D. Thesis, Eindhoven Univesity of Technology, Eindhoven, The Netherlands, 1992.